applied optics

Computational method for simulation of thermal load distribution in a lithographic lens

Xinfeng Yu,* Mingyang Ni, Dawei Rui, Yi Qu, and Wei Zhang

State Key Laboratory of Applied Optics, Changchun Institute of Optics, Fine Mechanics and Physics, Chinese Academy of Sciences, Changchun 130033, China
**Corresponding author: yu_xfeng@126.com*

Received 9 March 2016; revised 28 April 2016; accepted 29 April 2016; posted 29 April 2016 (Doc. ID 260652); published 18 May 2016

As a crucial step for thermal aberration prediction, thermal simulation is an effective way to acquire the temperature distribution of lenses. In the case of rigorous thermal simulation with the finite volume method, the amount of absorbed energy and its distribution within lens elements should be provided to guarantee simulation accuracy. In this paper, a computational method for simulation of thermal load distribution concerning lens material absorption was proposed based on light intensity of lens elements' surfaces. An algorithm for the verification of the method was also introduced, and the results showed that the method presented in this paper is an effective solution for thermal load distribution in a lithographic lens.

OCIS codes: (170.0110) Imaging systems; (170.3010) Image reconstruction techniques; (170.3660) Light propagation in tissues.

http://dx.doi.org/10.1364/AO.55.004186

1. INTRODUCTION

Over the past decades, throughput and resolution of lithographic exposure tools have been continually improved due to the manufacturing demands of integrated circuits. Two ways are mainly introduced into industry to realize the above enhancements: increase of exposure dose and use of extreme off-axis illumination. However, an obvious problem referred to as thermal aberration arises by using these technologies [1–7]. On one hand, the increase of the exposure dose leads to more energy absorption by lens optical materials and coatings, resulting in a higher temperature in the lens elements. On the other hand, the off-axis illumination heats up the lens locally and enhances the inhomogeneous temperature distribution of the lens elements. The refractive index of optical materials varies with temperature, so the increase of temperature and the thermal inhomogeneity will lead to image degradation of the projection lens during the exposure process, such as defocus and distortion.

The usual technique to compensate for the lower order thermal aberrations mentioned above is to reposition certain lens elements up and down. Other advanced lens compensators, such as infrared aberration control [1,2] and adaptive lens elements [8], are also integrated in recent projection lenses to compensate for astigmatism caused by dipole illumination or other optical settings. The latest numerical aperture (NA) 1.35 immersion system applies a high-resolution wavefront manipulator called FlexWave with correction capability of the Zernike series up to 64 terms [9].

Since the amplitudes and components of thermal aberrations highly depend on the illumination conditions, mask patterns, and the interaction between them, thermal aberrations should be controlled by lens manipulators in real time to guarantee the throughput and resolution in different production processes [2,10]. Thus, accurate prediction of thermal aberration varying with time needs to be done to get feed-forward parameters for real-time compensation [11,12]. Besides, assessments of the severity of the thermal aberration issues according to the specific exposure schemes should also be performed by simulations, which are indispensable and provide a basis for the calibration and correction strategies during the design stage [12]. Thus, the thermal aberration prediction is not only critical for the projection lens design but also indispensable for the feed-forward process control in exposing the status.

However, thermal aberration can be accurately predicted only if the thermal load distribution can be precisely described according to a specified setting of the illumination condition and the mask pattern. The source of the thermal load within the objective lens can be divided into two categories: the lens material absorption and the optical coatings absorption. By illumination simulation using LightTools (LightTools is a trademark of Synopsys, Inc.), we can achieve the energy absorbed by the optical materials and coatings and thus the laser beam intensity distribution on the lens surfaces. However, due to the limitation of LightTools itself, the thermal load distribution concerning lens material absorption could not be achieved directly. In the case of a rigorous thermal simulation with the

finite volume method, lacking the thermal load distribution will lead to an incorrect distribution of temperature, which will further affect the thermal aberration prediction. How to deal with the thermal load distribution of projection lenses is rarely mentioned in previous research. In this paper, a new computational method for the simulation of thermal load distribution concerning the material absorption was developed according to the light intensity distribution on lens element surfaces. Since the method is just an approximation of the actual thermal load distribution, its accuracy was also evaluated.

2. HEAT ABSORPTION RATE FORMULAS

Beam intensity decreases due to the light absorption and scattering as the light from the laser travels through optical elements. The laser beam intensity I after the traveling distance l can be expressed as follows [13]:

$$I = I_0 e^{-(\alpha_a+\alpha_s)l}, \tag{1}$$

where α_a is the absorption coefficient, α_s is the scattering coefficient, and I_0 is the incident light intensity.

The light intensity varies with the propagation distance as depicted in Eq. (1), which is derived under the hypothesis of a monochromatic plane wave traveling through homogeneous material. Due to the complexity of the light paths within the lithographic lens, some simplifications have to be made beforehand.

Referring to Fig. 1, we make the approximation that light paths through any lens element of a lithographic lens are determined by the entrance and exit lens apertures and are rotationally symmetric about the longitudinal axis [14]. This is different from real light paths in actual circumstances. However, this definition will fulfill the thermal load distribution calculation after some appropriate treatments.

We denote $(R_{\text{in}}, \theta_{\text{in}}, Z_{\text{in}})$ and $(R_{\text{out}}, \theta_{\text{out}}, Z_{\text{out}})$ as the coordinates of the incident point and the exit point, respectively, of a certain light path expressed in cylindrical coordinates, as shown in Fig. 1. The longitudinal coordinates Z_{in} and Z_{out} are functions of R_{in} and R_{out}, respectively, and can be calculated using the sag equation according to the surface parameters. Using the approximation above, it can be easily inferred that

$$R_{\text{out}} = R_{\text{in}} A_{\text{out}}/A_{\text{in}}, \qquad \theta_{\text{in}} = \theta_{\text{out}}, \tag{2}$$

where A_{in} is the semi-aperture of the entrance surface, and A_{out} is the semi-aperture of the exit surface.

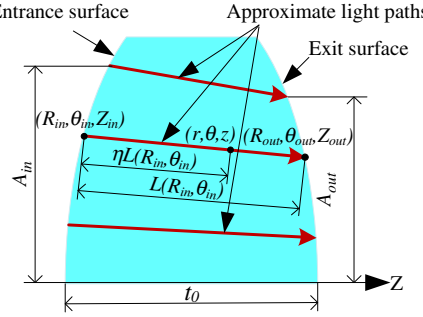

Fig. 1. Schematic illustration of approximate light paths in the projection lens element.

The propagation distance of the light path within the lens element, as shown in Fig. 1, is given by

$$L(R_{\text{in}}, \theta_{\text{in}}) = [(Z_{\text{out}} + t_0 - Z_{\text{in}})^2 + (R_{\text{in}} - R_{\text{out}})^2]^{\frac{1}{2}}, \tag{3}$$

where t_0 is the center thickness of the lens element. From Eqs. (2) and (3), we can deduce that the propagation distance L is just a function of R_{in} and θ_{in}.

The parameter η represents the proportion of the partial propagation distance of an arbitrary point inside the lens element to the total propagation distance given by Eq. (3). The proportion η ranges from 0 to 1. In the cylindrical coordinate system, the location of a point determined by η is given by

$$\begin{aligned} r &= \eta R_{\text{out}} + (1-\eta) R_{\text{in}}, \\ \theta &= \theta_{\text{in}}, \\ z &= (1-\eta) Z_{\text{in}} + \eta (Z_{\text{out}} + t_0), \end{aligned} \tag{4}$$

where (r, θ, z) are the coordinates of the point on the approximate light path, as shown in Fig. 1. Obviously, the point depicted in Eq. (4) is $\eta L(R_{\text{in}}, \theta_{\text{in}})$ away from the incident point and $(1-\eta)L(R_{\text{in}}, \theta_{\text{in}})$ away from the exit point. With Eq. (1), we can calculate the heat absorption rate of the point (r, θ, z) based on the entrance surface light intensity by

$$h_{\text{in}}(r, \theta, z) = C_1(r, \theta, z) \alpha_a I_{\text{in}}(R_{\text{in}}, \theta_{\text{in}}) e^{-(\alpha_a+\alpha_s)\eta L(R_{\text{in}}, \theta_{\text{in}})} \tag{5}$$

and the exit surface light intensity by

$$h_{\text{out}}(r, \theta, z) = C_2(r, \theta, z) \alpha_a I_{\text{out}}(R_{\text{out}}, \theta_{\text{out}}) e^{-(\alpha_a+\alpha_s)(1-\eta) L(R_{\text{in}}, \theta_{\text{in}})}, \tag{6}$$

where $I_{\text{in}}(R_{\text{in}}, \theta_{\text{in}})$ and $I_{\text{out}}(R_{\text{out}}, \theta_{\text{out}})$ are the light intensities of the incident point and exit point on the lens surfaces, respectively, and C_1 and C_2 are the coefficients referring to the cross-sectional area change of the laser beam during propagation and details of them will be discussed later.

In order to simulate the heat absorption rate more precisely, we calculate the heat absorption rate of the point (r, θ, z) by

$$h(r, \theta, z) = (1-\eta) h_{\text{in}}(r, \theta, z) + \eta h_{\text{out}}(r, \theta, z). \tag{7}$$

With weighted coefficients $1-\eta$ and η, the light intensities on both the entrance surface and the exit surface are considered. Since the light intensity distribution on lens surfaces obtained by illumination simulation is accurate, the heat absorption rate calculated in this way would be closer to the actual circumstances.

3. GENERATION OF THERMAL LOAD DISTRIBUTION

When a lens element's clear apertures are determined, the heat absorption rate defined in Eq. (7) can be expressed as a function of the incident point's coordinates $(R_{\text{in}}, \theta_{\text{in}}, Z_{\text{in}})$, the parametric variable η, and the light intensity on lens surfaces. According to thermal simulation software with the finite volume method, the thermal load distribution can be applied with a series of discrete points' coordinates and corresponding heat absorption rates. The generation of discrete points within the lens element by Eq. (4) can be outlined as follows. First, define the incident points' coordinates $(R_{\text{in}}, \theta_{\text{in}}, Z_{\text{in}})$ of the entrance surface. Generate a $n \times n$ grid mesh in the Cartesian coordinate system

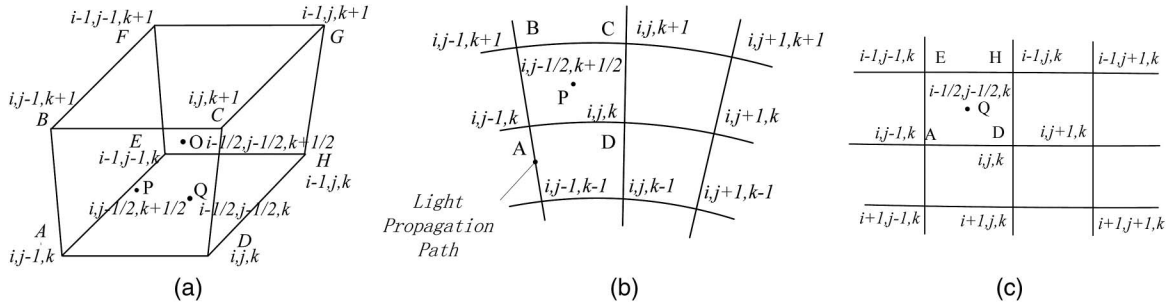

Fig. 2. Schematic illustration of the discrete point of the lens. (a) Hexahedron element, (b) the ith section, and (c) the kth section.

according to the aperture of the entrance surface and wipe off points located outside the clear aperture. Convert the Cartesian coordinates into polar coordinates and obtain Z_{in} by the sag equation. Until now, the coordinates of the incident points $(R_{\text{in}}, \theta_{\text{in}}, Z_{\text{in}})$ are defined. By taking a series of values from the parametric variable η, the discrete points in the lens element are created using Eq. (4). All the light paths determined by the different incident points adopt the same values from η. Thus, all the discrete points within the lens element are determined.

A schematic illustration of the discrete points in the lens element is shown in Fig. 2. Figure 2(a) shows a hexahedron defined by eight adjacent discrete points. Figures 2(b) and 2(c) show the ith section and the kth section of discrete points, respectively. For convenience, as shown in Fig. 2, we labeled each point, surface, and hexahedron. Point D is labeled by (i, j, k). Point P is the center of quadrangle ABCD and is labeled by $(i, j - 1/2, k + 1/2)$. Point O is the center of hexahedron ABCDEFGH and is labeled by $(i - 1/2, j - 1/2, k + 1/2)$. We use the index of point P to represent the index of quadrangle ABCD and the index of point O to represent the index of hexahedron ABCDEFGH. Following the same numbering scheme, all points, surfaces, and hexahedrons can be labeled.

The direction of the line DC is the approximate direction of the light path. C_1 and C_2 in Eq. (7) are related to the cross-sectional area change of the laser beam during propagation. Thus, C_1 and C_2 at point D can be calculated by

$$C_{1_{i,j,k}} = S_{i,j,1}/S_{i,j,k},\ C_{2_{i,j,k}} = S_{i,j,k_{\max}}/S_{i,j,k}, \tag{8}$$

where $S_{i,j,k}$ is the projection area perpendicular to the ray direction and can be given as follows:

$$S_{i,j,k} = \frac{1}{4}\left(\vec{S}_{i-\frac{1}{2},j-\frac{1}{2},k} + \vec{S}_{i-\frac{1}{2},j+\frac{1}{2},k} + \vec{S}_{i+\frac{1}{2},j-\frac{1}{2},k} + \vec{S}_{i+\frac{1}{2},j+\frac{1}{2},k}\right) \bullet \vec{k}_{i,j}, \tag{9}$$

where $\vec{S}_{i-1/2,j-1/2,k}$, $\vec{S}_{i-1/2,j+1/2,k}$, $\vec{S}_{i+1/2,j-1/2,k}$, and $\vec{S}_{i+1/2,j+1/2,k}$ are the area vectors around point D, and $\vec{k}_{i,j}$ is the unitary light path direction of point D.

By Eqs. (2)–(9), all the heat absorption rates of the discrete points generated above can be calculated. Thus, with all the discrete points' coordinates and corresponding heat absorption rates, thermal simulation can be performed.

4. METHOD OF VERIFICATION

As mentioned above, the light paths we defined do not correspond to the real light paths that travel through the lens. Although this has been considered in Eq. (7), the reasonableness of this method and its difference from actual circumstances should be verified.

Using LightTools, energy absorbed by the lens material can be obtained, but the heat absorption rate cannot be extracted. Our verification is based on the comparison of the absorbed energy calculated by our formulas and that given by LightTools.

As described above, it is convenient to calculate the absorbed energy of the lens element by numerical integration by decomposing the lens element into small hexahedrons with discrete points used for heat absorption rate calculation. Thus, we have

$$E = \sum_i \sum_j \sum_k h_{i-\frac{1}{2},j-\frac{1}{2},k+\frac{1}{2}} \times V_{i-\frac{1}{2},j-\frac{1}{2},k+\frac{1}{2}}, \tag{10}$$

where $h_{i-1/2,j-1/2,k+1/2}$ is the heat absorption rate of the hexahedron shown in Fig. 2(a), and $V_{i-1/2,j-1/2,k+1/2}$ is the hexahedron's volume. The heat absorption rate of the hexahedron is estimated by averaging the heat absorption rates of the eight points around point O as

$$h_{i-\frac{1}{2},j-\frac{1}{2},k+\frac{1}{2}} = \frac{1}{8}(h_{i,j,k} + h_{i,j-1,k} + h_{i,j-1,k+1} + h_{i,j,k+1} + h_{i-1,j,k} + h_{i-1,j-1,k} + h_{i-1,j-1,k+1} + h_{i-1,j,k+1}), \tag{11}$$

where $h_{i,j,k}$, $h_{i,j-1,k}$, $h_{i,j-1,k+1}$, $h_{i,j,k+1}$, $h_{i-1,j,k}$, $h_{i-1,j-1,k}$, $h_{i-1,j-1,k+1}$, and $h_{i-1,j,k+1}$ are the heat absorption rates of points D, A, B, C, H, E, F, and G, and they can be calculated by Eq. (7).

The volume of the hexahedron can be obtained by the following Gauss formula:

$$V = \iiint_V \left(\nabla \bullet \frac{\vec{x}}{|x|}\right) \mathrm{d}V = \iint \frac{\vec{x}}{|x|} \bullet \mathrm{d}\vec{S} = \sum_{n=1}^{6} \frac{\overrightarrow{x_{cn}}}{|x_{cn}|} \bullet \overrightarrow{S_n}, \tag{12}$$

where x_{cn} refers to the coordinate of the nth surface center of a hexahedron, and S_n denotes the area of the corresponding surface.

5. ANALYSES AND COMPARISONS OF ABSORBED ENERGY FROM DIFFERENT PROJECTION LENSES UNDER DIFFERENT ILLUMINATION CONDITIONS

Simulation accuracy of the thermal load distribution is demonstrated by a dioptric projection lens with NA 0.75 [15], as shown in Fig. 3(a), and a catadioptric projection lens with NA 1.20 [16], as shown in Fig. 3(b). The working wavelength of these two optical systems is 193.368 nm. The maximum root mean square (RMS) values of wavefront error of the dioptric projection lens and catadioptric lens are less than 0.6 nm and 0.8 nm, respectively.

Two kinds of materials are used in these lithographic lenses. Elements in gray color are made of CaF_2 and others are made of quartz. The main purpose of using CaF_2 in the lens elements close to aperture is to reduce the chromatic longitudinal error. However, the CaF_2 lens element next to the wafer does not help in terms of chromatic longitudinal error but is necessary to prevent compaction [17]. The main properties of the materials used for the simulation of thermal load distribution are presented in Table 1.

Light diffracted and blocked by the mask patterns significantly alter the light intensity distribution on the lens surfaces. For simplification, a blank retile was applied in our verification. Four illumination conditions were adopted, including conventional illumination, annular illumination, dipole illumination, and quadrupole illumination. Table 2 gives the illumination conditions used for the simulation of the thermal load distribution. The average power at the wafer is scaled to 0.3 W for all the different simulation cases.

Figure 4 shows the simulated heat absorption rate distribution under the annular illumination in the meridional plane of

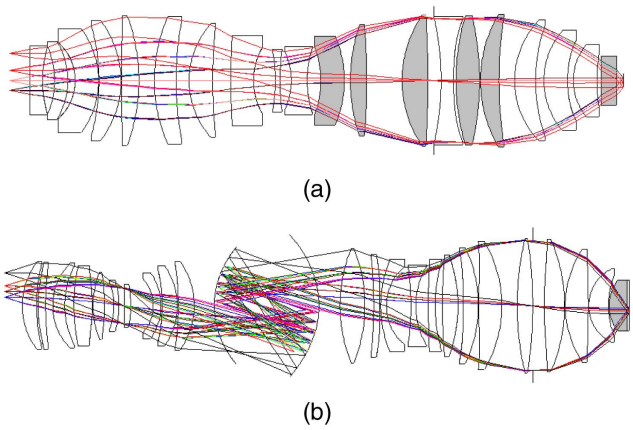

Fig. 3. Lithographic lenses used for the thermal load distribution calculation. (a) A NA 0.75 projection lens. (b) A NA 1.20 projection lens.

Table 1. Relevant Properties of Lens Materials

	α_a (10^{-4}/mm)	α_s (10^{-4}/mm)
Quartz	2.07	1.38
CaF_2	1.50	1.50

Table 2. Illumination Conditions for the Simulation of Thermal Load Distribution

Illumination Type	NA/σ_{in}/σ_{out} Dioptric Projection Lens	NA/σ_{in}/σ_{out} Catadioptric Projection Lens	Average Power at Wafer/W
Conventional	0.75/0/0.80	1.20/0/0.93	0.3
Annular	0.75/0.65/0.89	1.20/0.76/0.96	0.3
Dipole-X 35°	0.75/0.65/0.89	1.20/0.76/0.96	0.3
Quadrupole-45° 35°	0.75/0.65/0.89	1.20/0.60/0.80	0.3

the projection lens. Considering the light paths in the lithographic lens under annular illumination, our formulas give a reasonable description of the heat absorption rate, except for the last lens element of the catadioptric projection lens. The heat absorption rate distribution of the last lens element of the catadioptric projection is not reasonable since a higher heat absorption rate appears in the region where the light might not travel through. This error is the consequence of the approximate light paths used in our method, especially in the catadioptric projection lens with an off-axis field.

Figure 5 shows the comparison of the absorbed energy of the dioptric projection lens obtained by our formulas and by LightTools. Among all the four illumination conditions, absorbed energy obtained by our formulas is slightly lower than that by LightTools for most lens elements, and the energy differences range from –6.7% to 1.5%. Comparing simulation errors of all the lens elements of two different materials, the average simulation error of the CaF_2 lens elements is larger than that of quartz lens elements. Through the results of this dioptric projection lens, we still could not make a distinction about whether it is caused by the material properties or by our formulas. Thus, further investigation should be continued on this problem. However, the errors are still acceptable despite larger errors in CaF_2 elements.

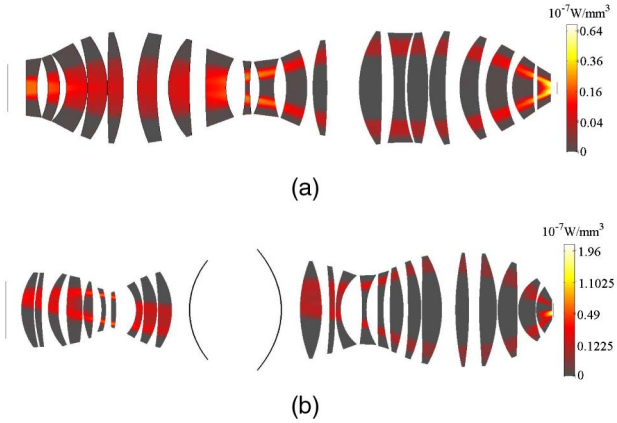

Fig. 4. Simulated heat absorption rate in the meridian plane of the projection lens under annular illumination. (a) The NA 0.75 projection lens. (b) The NA 1.20 projection lens.

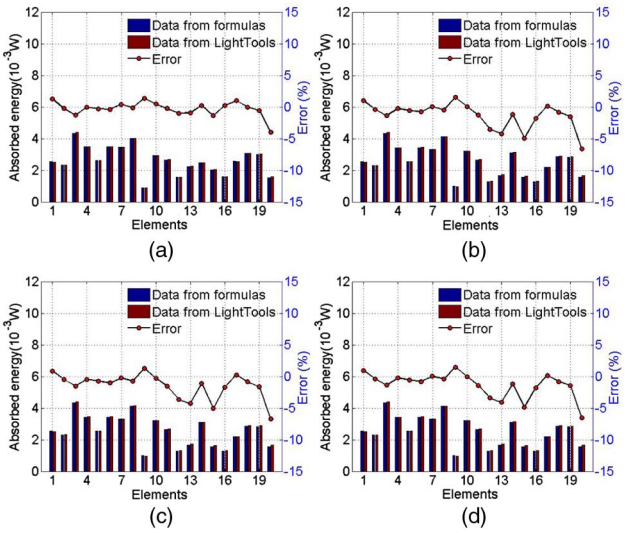

Fig. 5. Comparison of energy absorbed by the NA 0.75 projection lens from heat absorption rate formulas and LightTools. (a) Conventional illumination. (b) Annular illumination. (c) Dipole illumination. (d) Quadrupole illumination.

Results of the catadioptric projection lens are shown in Fig. 6. The simulation errors range from −12.0% to 5.9% for all simulation cases. It should be noted that the element numbers shown in Fig. 6 only refer to the refractive lens elements. It can be easily found that the last lens element of the catadioptric lens gives larger simulation errors. Referring to Fig. 4(b), we think it is the unreasonable heat absorption rate contributing more to the errors rather than the application of CaF_2. Similarly, the same holds for the last lens element of the dioptric projection lens.

Considering the results of different illumination conditions with the same partial coherence factor, such as annular, dipole, and quadrupole illuminations for the dioptric lens projections shown in Figs. 5(b)–5(d), respectively, the absorption energy and simulation errors for different lens elements are almost the same. This also holds for the results of the catadioptric lens shown in Figs. 6(b) and 6(c). The partial coherence factor decides the radial distribution of the light intensity on the element surfaces. Though the circumferential distribution of the light intensity on the lens surfaces varies under different illumination conditions, the rotational symmetry of the lens elements balances out this influence and keeps the same amount of absorbed energy. Our approximate light paths are also rotationally symmetric about the optical axis, so the same simulation errors appear under different illumination conditions. For different partial coherence factors, the absorbed energy and simulation errors are different. If we define the average partial coherence factor as $\sigma_{avg} = (\sigma_{in} + \sigma_{out})/2$, we would find that a larger average partial coherence factor would lead to larger simulation errors, such as conventional, dipole, and quadrupole illumination of the catadioptric lens elements shown in Figs. 6(a), 6(c), and 6(d), respectively.

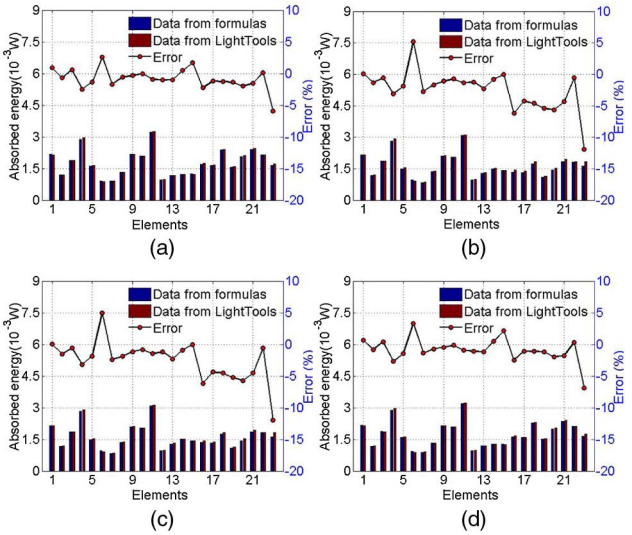

Fig. 6. Comparison of energy absorbed by the NA 1.2 projection lens from heat absorption rate formulas and LightTools. (a) Conventional illumination. (b) Annular illumination. (c) Dipole illumination. (d) Quadrupole illumination.

Comparing the results of the two different lithographic lenses, we can conclude that our method gives better results for lithographic lenses with smaller numerical apertures and on-axis fields. Nevertheless, during the simulation, the thermal load distribution and amplitude are provided separately. In such case, the amount of absorbed energy can be precisely provided, which makes the calculation error even smaller. Thus, the method for the simulation of thermal load distribution developed in this paper would be an effective solution for the thermal aberration prediction of the projection lenses.

6. CONCLUSIONS

This paper presents a solution for the simulation of the thermal load distribution due to lens material absorption. We first developed the light paths determined by the entrance and exit lens apertures. Thus, we can simplify the complex light paths that travel in the lithographic lens. Based on such simplification, the heat absorption rate formulas were given considering light intensity on both the entrance and exit surfaces. A method for generating the thermal load distribution was also provided according to the thermal simulation software demands. Two kinds of projection lenses under four illumination conditions were adopted to test the reasonableness of our method. The amount of energy calculated by our heat absorption rate formulas is in good agreement with that given by the illumination simulation for most lens elements. The simulation errors of the absorbed energy range from −6.7% to 1.5% and −12.0% to 5.9% for different lens elements of the dioptric lens and catadioptric lens, respectively. The results show that the heat absorption rate formulas introduced in this paper give smaller errors in low-NA projection lenses. Considering the simulation error, this method provides us with an acceptable solution to deal with the thermal load distribution calculation for the thermal aberration prediction in lithographic lenses and other similar optical systems.

Funding. National Science and Technology Major Project of China (2009ZX02205).

REFERENCES

1. Y. Uehara, T. Matsuyama, T. Nakashima, Y. Ohmura, T. Ogata, K. Suzuki, and N. Tokuda, "Thermal aberration control for low k1 lithography," Proc. SPIE **6520**, 6d205 (2007).
2. T. Nakashima, Y. Ohmura, T. Ogata, Y. Uehara, H. Nishinaga, and T. Matsuyama, "Thermal aberration control in projection lens," Proc. SPIE **6924**, 69241 (2008).
3. T. Yoshihara, T. Sukegawa, N. Yabu, M. Kobayashi, T. Arai, T. Kitamura, A. Shigenobu, Y. Hasegawa, and K. Takahashi, "Advanced aberration control in projection optics for double patterning," Proc. SPIE **7274**, 72741 (2009).
4. Y. Ohmura, T. Ogata, T. Hirayama, H. Nishinaga, T. Shiota, S. Ishiyama, S. Isago, H. Kawahara, and T. Matsuyama, "An aberration control of projection optics for multi-patterning lithography," Proc. SPIE **7973**, 79730 (2011).
5. Q. Zhang, K. Poolla, and C. J. Spanos, "Modeling of mask thermal distortion and its dependency on pattern density," Proc. SPIE **5853**, 234–242 (2005).
6. A. Chiba, K. Ota, T. Ogawa, and S. Okazaki, "Thermal distortion model of mask for extreme ultraviolet lithography during periodic scanning exposure," in *Proceedings of IEEE International Conference on Microprocesses and Nanotechnology* (IEEE, 2001), pp. 124–125.
7. V. V. Zelenogorsky, A. A. Solovyov, I. E. Kozhevatov, E. E. Kamenetsky, E. A. Rudenchik, O. V. Palashov, D. E. Silin, and E. A. Khazanov, "High-precision methods and devices for in situ measurements of thermally induced aberrations in optical elements," Appl. Opt. **45**, 4092–4101 (2006).
8. J. Mulkens, J. Klerk, M. Leenders, F. Jong, and J. W. Cromwijk, "Latest developments on immersion exposure systems," Proc. SPIE **6924**, 69241 (2008).
9. F. Staals, A. Andryzhyieuskaya, H. Bakker, M. Beems, J. Finders, T. Hollink, J. Mulkens, A. Nachtwein, R. Willekers, P. Engblom, T. Gruner, and Y. Zhang, "Advanced wavefront engineering for improved imaging and overlay applications on a 1.35 NA immersion scanner," Proc. SPIE **7973**, 79731 (2011).
10. P. Liu, M. Snajdr, X. Zhang, Y. Cao, J. Ye, and Y. Zhang, "A computational method for optical application specific lens control in microlithography," Proc. SPIE **7640**, 76400 (2010).
11. J. Bekaert, L. Van Look, G. Vandenberghe, P. van Adrichem, M. J. Maslow, J. W. Gemmink, H. Cao, S. Hunsche, J. T. Neumann, and A. Wolf, "Characterization and control of dynamic lens heating effects under high volume manufacturing conditions," Proc. SPIE **7973**, 79730 (2011).
12. K. Fukuhara, A. Mimotogi, T. Kono, H. Aoyama, T. Ogata, N. Kita, and T. Matsuyama, "Solutions with precise prediction for thermal aberration error in low k1 immersion lithography," Proc. SPIE **8683**, 86830 (2013).
13. P. R. Yoder, *Opto-Mechanical Systems Design* (Academic, 2006).
14. SigFit Reference Manual, version 2012R1d, Sigmadyne Inc.
15. Y. Omura, "Projection exposure methods and apparatus, and projection optical systems," U.S. patent 6,864,961 B2 (8 March 2005).
16. D. Shafer, W. Ulrich, A. Dodoc, R. V. Buenau, H.-J. Mann, and A. Epple, "Catadioptric projection objective," U.S. patent 8, 339,701 B2 (25 December 2012).
17. W. Ulrich, S. Beiersdorfer, and H.-J. Mann, "Trends in optical design of projection lenses for UV and EUV lithography," Proc. SPIE **4146**, 13–24 (2000).